10035 words

Wool waste used as sustainable nonwoven for building applications

Chiara Rubino [a,] *, Marilés Bonet Aracil [b], Stefania Liuzzi [a], Pietro Stefanizzi [a] and Francesco Martellotta[a]

[a] Dipartimento di Scienze dell'Ingegneria Civile e dell'Architettura, Politecnico di Bari, via Orabona 4, I-70125 Bari, Italy; chiara.rubino@poliba.it (C.R.); stefania.liuzzi@poliba.it (S.L.); pietro.stefanizzi@poliba.it (P.S.); francesco.martellotta@poliba.it (F.M.)

[b] Grupo de Investigación en la Industria Textil (GIITEX), Departamento de Ingeniería Textil y Papelera, Universitat Politècnica de València, 46022 Alcoy, Alicante, Spain; maboar@txp.upv.es (M.B.A.)

***** Corresponding author: chiara.rubino@poliba.it;

Abstract

Reusing textile waste in building applications has the potential to reduce the environmental impact of two sectors considered the main sources of environmental pollution: the textile and the construction industries. Thus, the main goal of the present research study is to assess the potential conversion of wool waste into new raw materials suitable for building components. Hence, hygrothermal, acoustic and non-acoustic properties of nonwovens consisting of 100% wool waste fibers thermally bonded with polyester/copolyester bi-component fibers were explored. Five different density values (51, 90, 115, 136 and 167 kg/m^3) were examined. Absorption coefficients ranging from 0.7 to almost 1 were measured above 1 kHz using 50 mm thick samples; thermal conductivity values from 0.044 to 0.057 W/(m·K) were obtained and a water vapour permeability close to $2 \cdot 10^{-11}$ kg/(m·s·Pa) was found. Furthermore, a comparison between nonwovens under test and other previously experimented materials was carried out. Measurement results showed that the manufacturing processes mainly affected the sound absorption coefficients and the hygric properties of the fibrous nonwovens. Comparison between tested materials and those currently available on the market allows to state that the tested nonwovens may represent a valid alternative for building applications, thus opening a new research area.

Keywords: textile waste recycling, bicomponent fibers as binder, thermal insulator, acoustic absorber.

c	specific heat capacity	J/kg·K
d	specimen thickness	m
e	mean absolute error of the sound absorption coefficients	-
D	thermal diffusivity	m^2/s

s	shape factor	-
α	sound absorption coefficient	-
δ	water vapour permeability	kg/m·s·Pa
ε	porosity	-
λ	thermal conductivity	W/m·K
Λ/Λ'	characteristic length ratio	-
μ	water vapour resistance factor	-
ρ_{bulk}	bulk density	kg/m^3
ρ_c	volumetric heat capacity	J/m^3·K
ρ_{true}	true density	kg/m^3
σ	air flow resistivity	kN·s/m^4
τ	tortuosity	-
*	values obtained using the inverse method	
D&B	values obtained using the Delany-Bazley method	
JCA	values obtained using the Johnson-Champoux-Allard method	

1. INTRODUCTION

Reusing and recycling waste materials represents an excellent opportunity to support a circular economy model in a society where resources are on the downgrade (Balador et al., 2020). Several waste (i.e. textiles) have not profitable recycling, despite their potential (Danihelová et al., 2019). The Circular Economy Package (Circular Economy Package, 2018) was adopted by the European community with the aim to impose the waste separation by 2025. Despite the policy measures, the implementation of circular economy in textile industries of some EU Member States is still very limited mainly due to the low economic viability (Leal Filho et al., 2019). Thus, an alternative solution to disposal could be the inclusion of waste into a new additional market, applying an open-loop recycling system (Payne, 2015). According to Muthu et al., (2012a), the market price of recycled fibers is generally lower than that of virgin ones (i.e. the ratio of the price of the recycled wool fibers versus that of virgin ones was 0.17), encouraging the possible investors in the use of textile cutoffs as secondary raw materials. Similar incentives might be applied in terms of cost of disposal. In fact, the present study was carried out in collaboration with a private company for which the cost of pre-consumer textile disposal (which is considered a special waste) was 70% higher than that of ordinary municipal waste.

Furthermore, the use of waste as new raw materials decreases the need for non-renewable resources. In fact, new synthetic fibers originated from petrochemicals are responsible for carbon dioxide emissions, but also vegetal and animal fibers (i.e. cotton or wool) generate environmental pollution due to the large use of land, water, fertilizers and pesticides (Sandin and Peters, 2018). Sandin et al., 2019 estimated that the greenhouse gas emissions associated with wool fibers production ranges from 1.7 kg CO_2 to 36.2 kg CO_2 equivalents per kg fibers. Differences in gas emissions for the production of wool could be affected by geographical location changes (Gowane et al., 2017). According to Muthu et al., (2012a), recycling and reuse practices may have environmental benefits resulting in about 16 kWh of energy saved for each kilogram of wool, but Muthu et al., (2012b) estimated the need to recycle at least 75% of pre-consumer waste to obtain a significant lowering of the carbon footprint of a textile product.

Considering the good thermal and acoustic performance expected from fibrous building materials, the textiles by-products represent a secondary opportunity to be used as new raw materials for the production of high efficiency building composites. In this way, it was possible to reduce the environmental effects of the construction phase which represent one of the most impacting phases of the life cycle of a building, consuming 30% of natural virgin resources (Bilal et al., 2020). Consumption of resources can be reduced by applying the circular economy principles and promoting more resource efficient methods to produce construction components (Munaro et al., 2020).

The production of textile building materials can be achieved using the fabrics directly, without converting them into fibers (i.e. direct methods); or converting the fabrics into fibers to form batting webs which are tied together by chemically gluing, mechanically entangling, or thermally bonding techniques (i.e. nonwovens). In terms of fabrication of nonwovens for building applications the number of systematic studies investigating hygro-thermal and/or acoustical properties is quite limited. Lee and Joo (2003) used low melting-point polyester to bond polyester waste fibers creating building nonwovens. El Wazna et al., (2019) produced textile waste nonwovens with promising thermal insulation properties (i.e. thermal conductivity values lower than 0.04 W/(m·K). Baccouch et al., (2020) investigated the acoustic properties of cotton, polyester and cotton/polyester nonwovens, obtaining a sound absorption coefficient higher than 0.4 above 500 Hz. A decrease of the acoustic performances (i.e. sound absorption coefficient lower than 0.2 above 500 Hz) was observed after blending nonwovens in epoxy resin. More systematic studies on this field are certainly lacking, while

many other types of waste have been used in combination with the different bonding techniques.

When dealing with the chemical binding method, several studies can be found in consequence of the fact that it is the easiest process as it only involves the application of binder dispersions followed by the curing and drying of the impregnated fibers (Wilson, 2006). By properly choosing the strength of the binder, different materials have been used to provide the fibrous matrix needed to ensure good thermal and acoustic performance. Khan et al., (2017) studied the acoustic properties of innovative materials made from recycled tyres mixed with different percentages of bio-binder. Recently, the use of vegetable fibers as matrix for building materials has become one of the trending research topic. Martellotta et al., (2018) and Liuzzi et al., (2020) investigated the use of olive tree-pruning waste to produce innovative panels with good hygrothermal and acoustic performances. Stefan de Carvalho et al., (2020), proposed the use of different sizes of sunflower residues mixed with plaster and sodium benzoate in order to obtain sustainable panels. One of the main issues of the sustainable materials can be considered by the scarce load-bearing performance (Nakanishi et al., 2018). A common issue with chemically bonded materials is represented by nature and amount of the binder which can clearly influence the porosity of the samples (and hence the properties depending on it), mechanical resistance, without neglecting the environmental impact of the binder, which is not always negligible.

From this point of view, a better alternative might be the needle-punching technique. It consists in a repeated penetration of barbed needles trough a preformed dry fibrous web (Anand et al., 2006). Materials with different density values could be produced controlling the density of the final products by varying the needle penetration depth (Muthukumar et al., 2017). Thus, panels with higher density showed better load-bearing properties, whereas materials with less density values favored acoustic absorption and thermal insulation (Cerkez et al., 2017).

The thermal bonding method involves the use of “base” fibers included in a polymer matrix working as “binder”. A carefully chosen mix of base and binder fibers is heated to melt the thermoplastic polymer and, then is cooled to solidify the bonding area. According to Pourmohammadi, (2006), the thermal bonding technique could be considered more economically attractive than chemical one because involved more energy savings as a

consequence of less water evaporation during bonding. Several authors (Hittini et al., 2019; Zhang et al., 2020) included waste materials in the polymer matrix to produce innovative building components. According to Islam and Bhat (2019), when thermoplastic fibers are used to bond cellulosic polymers, adopting a working temperature lower than that of degradation of cellulosic matrix is an important strategy. Ramamoorthy et al., (2014), analyzing different methods for recycling cotton/PET fabrics to produce building composites, found that the addition of plasticizers allows to lower the melting temperature of PET and to bind the cotton fibers without damaging their chemical structure.

A different solution consisted in the use of copolyester/polyester bi-component fibers as thermoplastic matrix. The bi-component fibers are defined as "extruding two polymers from the same spinneret with both polymers contained within the same filament" (Avcioglu Kalebek and Babaarslan, 2016). The two polymers can be extruded with different cross-section shapes in order to obtain several configurations i.e. core/shell, side by side, or island in the sea. Çelikel and Babaarslan, (2017) tested the acoustic properties of mats composed by spun bonded layers produced with bi-component fibers having two different cross-sections (i.e. round and trilobal). During heating, one polymer works as low melting component and softens to form the bond; while the other works as higher melting component maintains its shape and its structural integrity (Mochizuki and Matsunaga, 2016). To this purpose, the bi-component fibers are usually applied for self-bonding in nonwoven composites with the aim of using lower molding temperatures than the usual thermal molding process (Naeimirad et al, 2018). Drochytka et al., (2017) used bi-component fibers to bind polyester waste fibers producing building nonwovens with thermal and acoustic performances comparable to mineral rock wool panels. Samples with three different density values (65, 80, 95 kg/m^3) were produced and a thermal conductivity less than 0.06 W/(m·K) was measured. A sound absorption depending on bulk density was observed in higher frequency range between 1000 and 1600 Hz.

Given the limited number of systematic studies on the use of textile waste to produce building materials with thermally insulating and sound absorbing properties, the present research aims at investigating the benefits of thermal bonding to produce textile nonwoven materials. A matrix of copolyester/polyester (Co-PET/PET) bi-component fibers were mixed and carded with 100% wool waste fibers to obtain innovative building composites. Several samples with different bulk density values were manufactured and their hygrothermal and

acoustic performances were tested. Finally, the experimental results were used to compare physical properties among different innovative materials previously tested (Rubino et al., 2019a; 2019b). The materials chosen for comparison were prepared using chitosan and gum Arabic binders to bond 100% wool waste fibers. Furthermore, a statistical analysis was carried out in order to study how the manufacturing processes could have affected the hygrothermal and acoustic performances of the final products.

2. Materials

2.1 Raw materials

Wool fibers, 100% recycled, obtained by scouring and carding tailored cuttings produced by the Italian clothing company Gordon Confezioni srl. (Apulia, Italy) were used as base fibers, whereas a copolyester/polyester (Co PET/PET) sheath-core bi-component fiber was used as received, as a thermoplastic matrix. A standard poly (ethylene terephthalate) (PET) fiber (ISO 105-F4) was used to compare with the bi-component one. A microstructure analysis was carried out by using a Scanning Electron Microscope ZEISS, model ULTRA 55, in order to characterize the morphology of the two types of tested fibers. Fig. 1a shows the outermost layer of the wool fibers, highlighting their typical scaly surface. After the scrubbing and carding actions, the edges of the scales tend to be curved favoring the entanglement of the fibers (Tridico, 2009). Fig. 1b shows the SEM images of the cross section detail of the bi-component fibers allowing to clearly distinguish two different layers which prove the sheath-core structure of the cross section of the binder fibers. The fibers were cut after freezing in liquid nitrogen for a few minutes in order to reduce the possibility of deformation when they were broken. All fractured surfaces were sputter-coated with gold before testing.

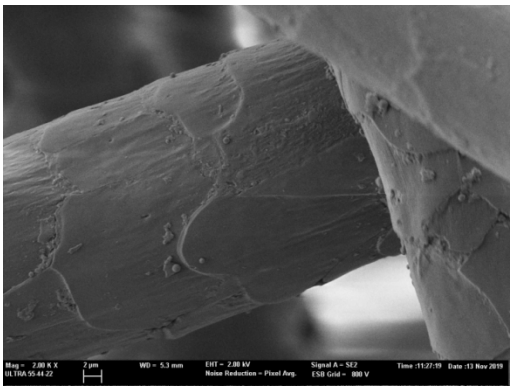

(a)

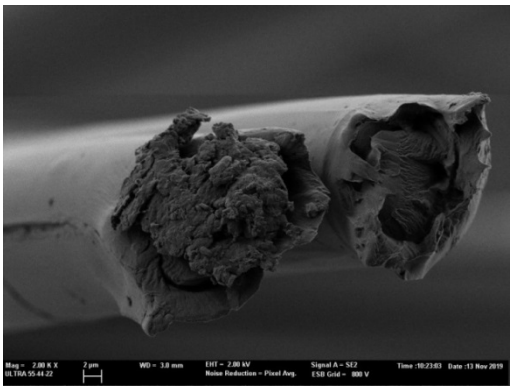

(b)

Fig. 1. Scaly outermost layer of the wool fibers at 2000X (a) and cross section of the Co-PET/PET bi-component fibers at 2000X (b).

A Differential Scanning Calorimetry (DSC) analysis was performed in order to characterize the thermal behaviour of the base and binder fibers. The aim was to choose the suitable working temperature to press the samples while avoiding the decomposition of the natural polymer and ensuring the melting of the synthetic ones. The analysis was carried out by using a DSC 1 Star System Mettler Toledo device, according to ISO 11357-1, (2016). Accurately weighted samples (2 mg each) were placed into aluminum pans and then crimped closed. A small hole was done on the top of the assembly in order to allow the release of water. An empty aluminum pan was used as a reference. During the experiments, the samples were heated from 30 °C to 350 °C for the bi-component fibers, and from 30 °C to 500 °C for the wool fibers. The temperature was increased at a heating rate of 30 °C/min and nitrogen was used as the purge gas at 50 ml/min.

Fig. 2 shows the DSC curve of wool in which two endothermic processes could be appreciated. The first endothermic process was approximately observed from 106 °C to 132 °C, with a peak temperature of 115 °C. It could be explained by the vaporization of the water as a consequence of the increasing temperature (Zargarkazemi et al., 2015). A second endothermic heat transfer was observed from about 253 °C to 426 °C. According to (Forouharshad et al., 2011), this baseline shift was related to α-keratin denaturation which involved the cleavage of the helical hydrogen bonds and the melting of the ordered regions of the wool. During this process, the breakdown of the disulfide bonds also occurred, causing the release of numerous volatiles i.e. hydrogen sulfide and sulfur dioxide.

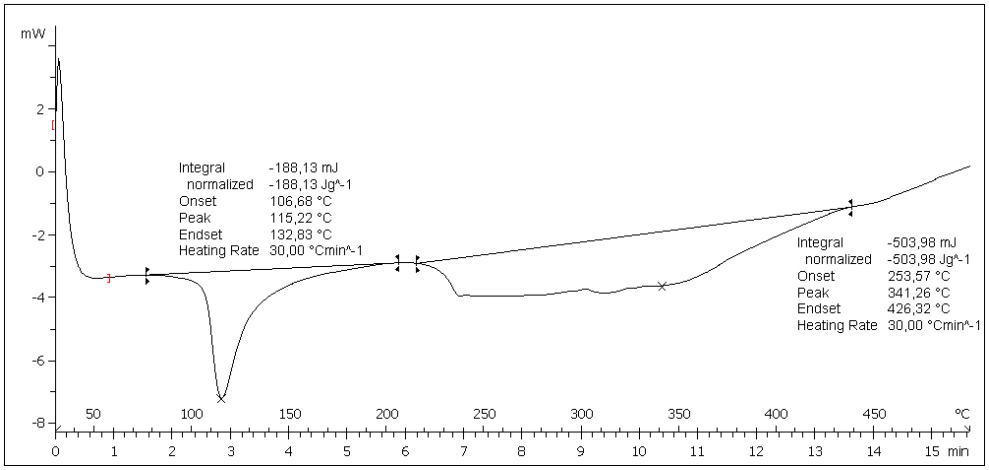

Fig. 2. DSC curve of 100% wool fibers obtained using nitrogen at 50 ml/min as purge gas.

The DSC curve of the synthetic fibers (Fig. 3) showed two endothermic baseline shifts which proved the presence of the two polymers. According to (Brydon and Pourmohammadi, 2006), the crystallites of the polyester melt at about 250 °C. Thus, it can be concluded that the first peak of the curve around 70 °C corresponded to the melting temperature of the copolyester polymer and the second peak around 253 °C was the melting temperature of the polyester.

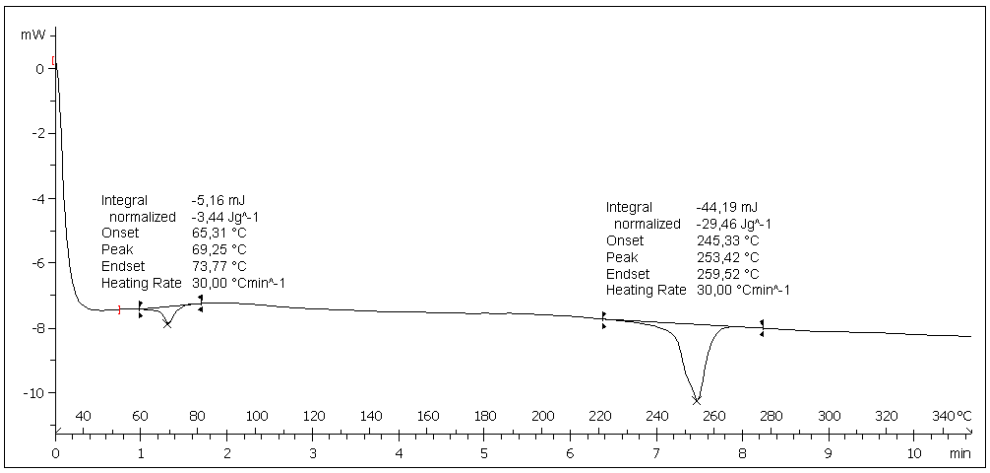

Fig. 3. DSC curve of copolyester/polyester sheath-core bi-component fibers obtained using nitrogen at 50 ml/min as purge gas.

The melting point at around 70 ºC is a low temperature for a polyester fiber, and it can be thought to be due to water presence on the fiber, similarly to wool. Polyester is a hydrophobic fiber and the moisture content will be lower than wool. However, the CoPET/PET analysis shows the peak centered at around 70 ºC and ends before 75 ºC. This makes us think it is not due to moisture but to the copolymer presence. PET melting temperature is centered around 255 ºC, and even if 70 ºC might seem to be too low for a polyester, it has been demonstrated that polymers such as poly (ethylene sebacate) have a melting temperature centered around 69.5 ºC (Wunderlich, 1980).

Bi-component fibers are focused on the purpose of melting at reduced temperatures so to avoid side effects such as yellowing, on the other fibers due to the temperature treatment. In order to confirm the fiber composition, the Fourier Transform Infrared Spectrum (FTIR) analysis was conducted. Fig. 4 shows the FTIR spectra for wool, CoPET/PET fiber and a standard PET (Poly-ethylene terephthalate). Samples were scanned with resolution of 4 cm^{-1}, 256 scans, at a range 400 to 4000 cm^{-1} using a JASCO FTIR 4700 equipped with an

Attenuated Total Reflectance (ATR). It can be clearly appreciated the difference between wool and polyesters. However, when the focus is placed on polyester, only slight differences can be observed between CoPET/PET fiber and a standard PET. Those alterations when compared to polyester spectrum may be attributed to the differences due to the new monomer included to obtain the copolymer CoPET.

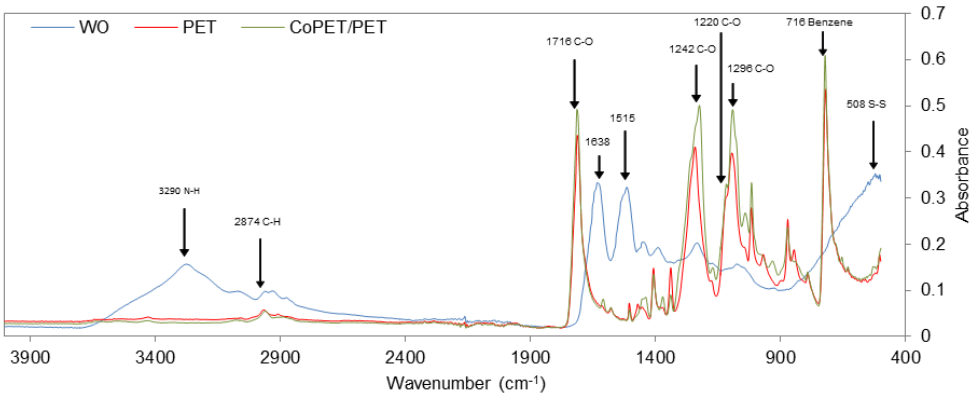

Fig. 4. FTIR analysis applied to the wool, PET and CoPET/PET fibers.

In Table 1, the difference between wool and polyesters, centered mainly in the bands showed in, is reported.

Table 1. Frequencies and assignments of bands identified in the FTIR spectra for PET and wool.

Frequency (cm^{-1})	Assigment	Fibre
508	S-S Stretching vibration	Wool (Wojciechowska et al. 2004, Pielesz et al., 2003)
1096	-C-O- vibration	PET (Li et al. 2004, Bozaci et al., 2012)
1120	-C-O- vibration	Wool and PET (Li et al. 2004, Bozaci et al., 2012)
1242	-C-O- vibration	PET (Li et al. 2004, Bozaci et al., 2012)
1515	-NH	Wool (Wojciechowska et al. 2004, Pielesz et al., 2003)
1638	-NH	Wool (Wojciechowska et al. 2004, Pielesz et al., 2003)
1717	-C=O stretching vibration	PET (Li et al. 2004, Bozaci et al., 2012)
2874	$-CH_2-$ stretching vibration	Wool and PET (Li et al. 2004, Bozaci et al., 2012)
3290	-NH	Wool (Wojciechowska et al. 2004, Pielesz et al., 2003)

Wool characteristic structure is the cysteine S-S bond; the S-S stretching vibration shows a characteristic band in the region 560-480 cm^{-1} (Wojciechowska et al., 2004). The N-H group, also characteristic from wool, can also be appreciated on the bands around 3290 cm^{-1}, 1638 cm^{-1} and 1515 cm^{-1} (Pielesz et al., 2003). Whereas the most characteristic peaks for PET are centered around 2874 cm^{-1} due to $-CH_2-$ groups; 1717 cm^{-1} due to carbonyl, C=O stretching vibration; 1242, 1120 and 1096 cm^{-1} are due to C-O vibration, and the ones between 900- 640

cm^{-1} which are the characteristic ones for benzene rings (Li and Ding, 2007; Zhang et al., 2008; Özdoğan et al., 2012).

2.2 Preparation of samples

Wool and bi-component fibers were thermally bonded to produce nonwoven materials. The compression molding technique was carried out by means of a hydraulic press built by Dupra SL company. The device was optimized by adjusting concentric metal cylinders on the two pressing plates (Fig. 5a). In detail, a hollow cylinder working as mold was fixed on the lower plate and another solid cylinder working as press was hooked on the upper plate. Molds with four different diameters (i.e. 10, 6 ,4 and 3 cm) were used in order to prepare samples with adequate sizes for testing the hygrothermal, acoustic and non-acoustic properties of the materials.

Defined proportions of wool and bi-component fibers were uniformly mixed, after being carded together. Then, several samples were prepared casting the fibrous blend in the cylindrical mold and pressing it by lowering the top plate up to a chosen height (5 cm for samples used to test the thermal, acoustic and non-acoustic properties and 1 cm for samples prepared to test the hygric properties). The fiber dosing of each specimen was controlled in terms of density. Five types of composites (subsequently referred as "BICO") with a bulk density ρ_{bulk} respectively equal to 51, 90, 115, 136 and 167 kg/m^3 were manufactured. The aim was to analyze the effects of such variations on sample porosity and, consequently, on the hygrothermal and acoustic performance of the final products.

The binder fibers content was chosen after producing samples having a fixed bulk density (0.51 kg/m^3) and bi-component fibers variable between 15 and 50% in mass. The percentage of 20% in mass was finally selected as it offered the best balance between porous structure and compactness of the skeleton.

As a consequence of the DSC results (Fig. 2-3), a temperature of 100 °C was chosen as working temperature. In this way, the best combination of the two synthetic polymers behaviors was performed. The compression molding process was applied for 1 hour, then the samples were cooled at environmental conditions.

3. Methods

3.1 Thermal properties

The thermal insulation properties of the BICO samples were experimentally investigated by means of the transient plane source device Isomet 2104 (Applied Precision Ltd). Two cylindrical specimens (5 cm thick and having a 10 cm diameter) for each type of material were tested placing the probe in two points of each sample surface and then assuming the average value as result. The tests were carried out at laboratory conditions of 21±2 °C and 45±5% RH. Thermal conductivity λ, thermal diffusivity D, and volumetric heat capacity ρ_c were provided from the analysis of the temperature response of the material as a consequence of the heat flow impulses induced by the resistor of the probe. The specific heat capacity c was calculated from the measured volumetric heat capacity and bulk density.

3.2 Hygric properties

The water vapour diffusion behaviour of the BICO samples was determined according to the EN 12086 (2013). The dry cup method was followed. Thus, two cylindrical samples for each type of material (1 cm thick and having a 10 cm diameter) were sealed on the top of PVC cups in which a relative humidity of 0÷4% was set by using a calcium chloride desiccant. The assemblies were then conditioned in the Angelantoni DY340 climatic chamber (Fig. 5b) at relative humidity of 50% and 23 °C and were daily weighed by a Mettler Toledo PB3002 (±0.01 g accuracy). The mass variations of the cups were recorded until weigh stabilization and the mass rate change G was determined by plotting mass gain as function of time. This was in order to calculate the water vapour permeance W which represents the ability of the different materials to transfer moisture due to a vapour pressure gradient ΔP between the two specimen faces.

$$W = G/(A \cdot \Delta P) \quad [1]$$

where A is the exposed area of the sample.
Thus, the water vapour permeability δ and the water vapour diffusion resistance factor μ, which are the commonly properties used to characterize the hygric behaviour of a building materials, were calculated as follows:

$$\delta = W \cdot d \quad [2]$$

$$\mu = \delta_{air}/\delta \quad [3]$$

where d is the sample thickness and δ_{air} is the water vapour permeability of air.

(a) (b)

Fig. 5. Hydraulic press used for compressing molding technique (a), sample conditioned in the climatic chamber for hygric measurements (b).

3.3 Non-acoustic properties

The open porosity (ε) was measured by a ULTRAPYC 1200-e Quantachrome Helium gas Pycnometer. During the measurement, the helium penetrated the smallest pores of the sample providing the value ρ_{true} of its true density. The ρ_{true} and ρ_{bulk} ratio was used to determine the open porosity ε of the investigated samples. Two cylindrical samples (5 cm thick and having a 4 cm diameter) were tested for each type of material.

Tortuosity is usually defined as the square of the ratio of actual flow path length to the straight distance between the ends of the flow path (Bear, 1988). The tortuosity τ of the studied materials was directly determined according to the Brown's method (Brown, 1980). Two samples (5 cm thick and having a 4 cm diameter) were tested for each density value, in order to evaluate how the arrangement of the pores influenced the path of a fluid through the different materials. The electrical resistivity of a BICO sample saturated of 10% $CuSO_4$ solution was determined after applying it an electrical current with a voltage variable from 1 to 8 voltage. The electrical resistivity of the conducting fluid was also calculated. The ratio between the two electrical resistivities was used to obtain the tortuosity values.

The air flow resistance σ_s of the investigated materials was experimentally evaluated according to the method proposed by Ingard and Dear, 1985. The measurement set up consisted in two methacrylate tubes of 4 cm inner diameter and 85 cm long, between which the tested sample was adjusted. The tube had two different terminations: a 5 cm loudspeaker

(Visaton FRS 5) with a frequency response spanning from 150 Hz to 20 kHz at one end and a rigid termination made by 5 cm thick methacrylate at the other end. The pressure drop of the fluid flow through the sample was extrapolated by acoustic measurements carried out using two microphones (Core Sound) with a flat frequency response from 20 Hz to 20 kHz and properly calibrated in amplitude and phase. The microphones were excited using an exponential sine sweep and located in front of the sample and in front of the rigid termination end. All the processing was repeated for two samples for each type of material.

3.4 Acoustic properties

The normal incidence sound absorption coefficients α were measured by means of a BSWA SW 260 two microphones impedance tube. It consisted of two parts: a tube with built-in loud speaker and a sample holder. According to ISO 10534-2, (1998), the transfer function method was performed to acquire the pressures produced by the sound source at two fixed microphones positions on the tube wall. The combination of measurement results derived from two different tube configurations (of different diameters and length) allowed to obtain the absorption coefficients in a wide frequency range (125 Hz – 6300 Hz). The first configuration considered the use of a tube with a 6 cm inner diameter of which used two different microphone spacing equal to 17 cm and 4.5 cm, respectively characterized by a low frequency limit of 800 and 2500 Hz. The second configuration involved replacing the sample holder with a 3 cm diameter extension. In this case, the microphone spacing was 2.25 cm resulting in a frequency range spanning between 800 Hz and 6300 Hz. Four samples 5 cm thick, two 6 cm e two 4 cm in diameter, were tested for each density value at laboratory conditions (21±2 °C). All processing was controlled by a VA-Lab IMP® software which played a 30 s unfiltered white noise signal.

3.5 Theoretical models

The measured sound absorption coefficients were compared with those predicted by the theoretical models. The empirical model proposed by Delany and Bazley (D&B) (Delany and Bazley, 1970) and the phenomenological model developed by Johnson, Champoux, and Allard (JCA) (Johnson et al.,1987; Allard and Champoux, 1992) were considered. The D&B model expresses the characteristic impedance and the wavenumber with simple power-law needing only the air flow resistivity σ (i.e. the air flow resistance per unit thickness) as input. More physical parameters were required to feed the JCA model which needed porosity ε,

tortuosity τ, viscous and thermal characteristic lengths Λ and Λ', and shape factor s, in addition to air flow resistivity. A more extensive explanation of the meaning of the physical parameters lays beyond the scope of this paper, therefore readers are referred to the original paper (Allard and Champoux, 1992) or textbooks (Cox and D'Antonio, 2004).

As it was impossible to measure all of the input parameters required by JCA model, an inverse method (Atalla and Panneton, 2005) was used to estimate the missing ones. Taking advantage of measured absorption coefficients, the values of the missing physical properties (i.e. viscous and thermal lengths ratio and shape factor) and of the directly measured ones (porosity, tortuosity and air flow resistivity), were determined by means of optimization techniques. A search algorithm was developed using the Matlab® software, in order to find the set of parameters which allowed the best match between measurements and predictions. The algorithm explored properties which were not measurable over the entire range of possible values, while for measured parameters the range chosen considering their average values and taking into account their uncertainty. As the porosity and tortuosity were characterized by very low uncertainty, their measured values were directly used as input data of the JCA model, allowing to speed up calculations. All the remaining input parameters, including air flow resistivity, which showed significant variations during measurements, were consequently estimated by the search algorithm. The air flow resistivity values resulting from the inverse method were also used to feed the Delany-Bazley model in order to get the best fit between measured and predicted absorption coefficients curves.

4. Materials chosen for comparison

The measurement results of BICO samples were finally compared with innovative materials obtained by binding similar 100% wool waste fibers with chitosan and gum Arabic solutions. Chitosan and gum Arabic based wool samples (respectively referred as CH and GA samples), whose thermal and acoustic behaviour were widely discussed in previously published works (Rubino et al., 2019a; 2019b), were further investigated in terms of hygric performances. The aim was to analyze the possible effects of the thermal and chemical manufactured process on the hygrothermal, acoustic and non-acoustic properties of the final nonwoven composites.

Cylindrical specimens (1 cm thick and having a 10 cm diameter) were made taking care to get final products with physical properties similar to those of the materials previously investigated (Rubino et al., 2019a; 2019b). Wool waste tailored cuttings belonging to the

same batch used to prepare the original samples (Rubino et al., 2019a; 2019b) were transformed into wool batting and uniformly mixed with chitosan and gum Arabic solutions, as outlined in Table 2.

Table 2. Details of the CH and GA samples (Rubino et al., 2019a; 2019b) used for the comparison with BICO samples.

Sample	Density	Composition
CH samples	CH-1_197 kg/m^3 CH-2_145 kg/m^3 CH-3_122 kg/m^3 CH-4_80 kg/m^3	40% wool fibrous matrix and 60% binder chitosan solution (15 g chitosan dissolved in 1000 g of water + 0.05 g of acetic acid)
GA samples	GA-1_177 kg/m^3 GA-2_143 kg/m^3 GA-3_93 kg/m^3	40% wool fibrous matrix and 60% binder gum arabic solution (200 g chitosan dissolved in 1000 g of water)

The fibers soaked in binder were casted in cylindrical molds and the blends dosing of each specimen was controlled by volume with a given density. Finally, the samples were dried in oven at 100 °C for one hour. CH samples with a density of 197, 145, 122 and 80 kg/m^3 and GA samples with a density of 177, 143 and 93 kg/m^3 were composed and tested with the same methodology described in Section 3.4.

5. Results and discussion

5.1 Morphological analysis

Fig. 6 shows the SEM images of the BICO samples obtained after applying the compression molding technique. The figure 6 highlights that the investigated materials consisted of an entanglement of wool and bi-component fibers with a random distribution. The result was a porous network in which the surface scale pattern distinguished the wool fibers from the smooth surface of the man-made polymers. Furthermore, it can be appreciated that the Co-PET/PET polymer were not completely melted and bonding points among fibers were obtained. Consequently, a high void fraction in the microstructure of the final product was preserved.

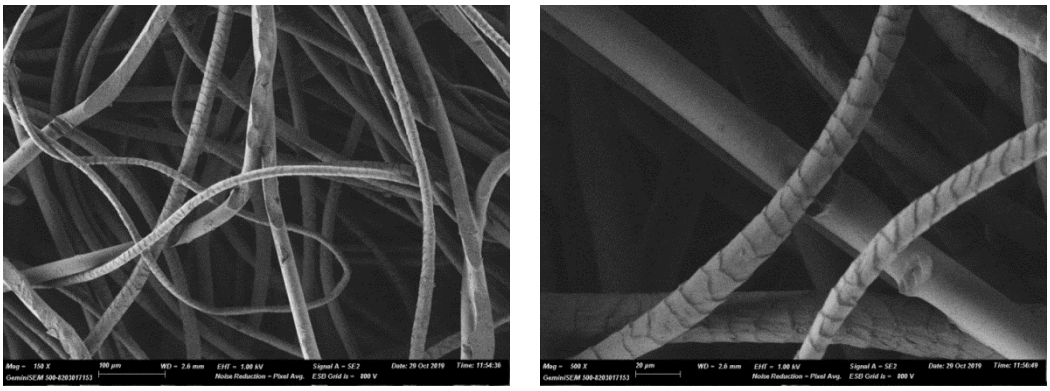

(a) (b)

Fig. 6. SEM images of BICO nonwoven materials at 150X (a) and 500X (b).

SEM images were analyzed using a Matlab® script and a population of 300 wool fibers was chosen in order to determine a distribution of their diameters. As shown in the bar chart in Fig. 7, fiber diameters ranged from 8 to 34 µm (with a mean value of 19 µm and a standard deviation of 7 µm). The diameters distribution of the bi-component fibers was also analyzed. They were characterized by a nearly constant diameter around of 22 µm as a consequence of their fabrication process. Although the mean diameters values of the wool and PET/CoPET fibers were very close, their distribution allowed to obtain high porous structure with positive effects on the hygrothermal and acoustic performances.

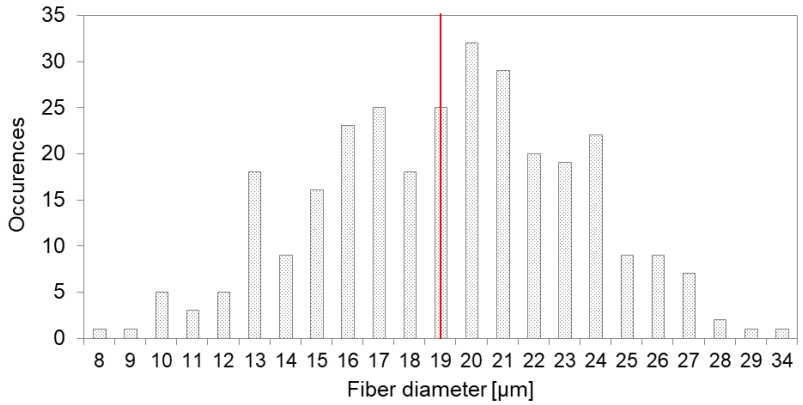

Fig. 7. Distribution of diameters of wool fibers. In red is reported the average fiber diameter value.

5.2 Hygrothermal properties

Table 3 summarizes the result of the thermal measurements for the materials produced using a Co-PET/PET fiber as binder. The experimental mean values of thermal conductivity, thermal diffusivity and specific heat capacity are given together with their measurement

uncertainty expressed as the standard deviation of the mean (GUM, 2008). The results achieved could be considered satisfactory, being in agreement with those obtained for bio-based insulating materials with similar density values, like panels made from hemp fibers and shives bonded with bi-component fibers (λ=0.044÷0.048 W/(m·K), ρ_{bulk}=33.1÷111.6 kg/m^3) or PLA (λ=0.037÷0.040 W/(m·K), ρ_{bulk}=40÷100 kg/m^3) and boards produced using a liquid glass to bind moss, rye straw and reed (λ=0.037÷0.056 W/(m·K), ρ_{bulk}=156÷191 kg/m^3) (Korjenic et al. 2016, Kremensas et al., 2017, Bakatovich et al., 2019). The experimental thermal conductivity values were also similar to those of thermal insulators based on mineral fibers (λ=0.054÷0.048 W/(m·K), ρ_{bulk}=40÷150 kg/m^3), cork (λ=0.043 W/(m·K), ρ_{bulk}=110÷160 kg/m^3) or perlite (λ=0.048 W/(m·K), ρ_{bulk}=80÷120 kg/m^3) (UNI 10351, 2015).

Table 3. Thermal properties of all tested materials by varying their density values ρ_{bulk}: mean values of thermal conductivity λ, thermal diffusivity D, specific heat capacity c and their standard deviation of the mean.

Tested materials	ρ_{bulk} [kg/m^3]	λ [W/(m·K)]	D [10^{-7}m^2/s]	c [J/(kg·K)]
BICO-1	167±6	0.057±0.0008	1.83±0.003	1863±22
BICO-2	136±1	0.054±0.0004	1.86±0.001	2148±6
BICO-3	115±1	0.052±0.0002	1.85±0.002	2459±7
BICO-4	90±2	0.050±0.0003	2.00±0.004	2770±10
BICO-5	51±1	0.044±0.0004	2.46±0.010	3544±13

In Fig. 8 a linear correlation between conductivity and density can be noted for all the compared materials. A regression analysis was performed to evaluate the statistical significance of the linear relationship between λ and ρ_{bulk}. For this reason, assuming a significance level $\alpha = 0.05$ and the relevant number of observations n for BICO, CH and GA samples ($n_{BICO} = 5$, $n_{CH} = 4$ and $n_{GA} = 3$), a hypothesis test of the slope of the regression lines β was applied using the Student's t distribution (Ortiz et al., 2009). The comparison between the statistic absolute values t_{calc} and the associated critical ones $t_{\alpha/2,(n-2)}$ (with n-2 degrees of freedom) was carried out to test the null hypothesis $\beta = 0$ versus the alternative one $\beta \neq 0$. The t_{calc} values computed for BICO, CH and GA samples were respectively 13.58, 26.82 and 29.89; while the associated critical values $t_{\alpha/2,(n-2)}$ were 4.18, 6.21 and 25.45. Being $|t_{calc}| > t_{\alpha/2,(n-2)}$ for each type of material, the null hypothesis was rejected at significance level α. Thus, a statistically significantly linear correlation between the independent variable ρ_{bulk} and the dependent variable λ was found for the three types of materials.

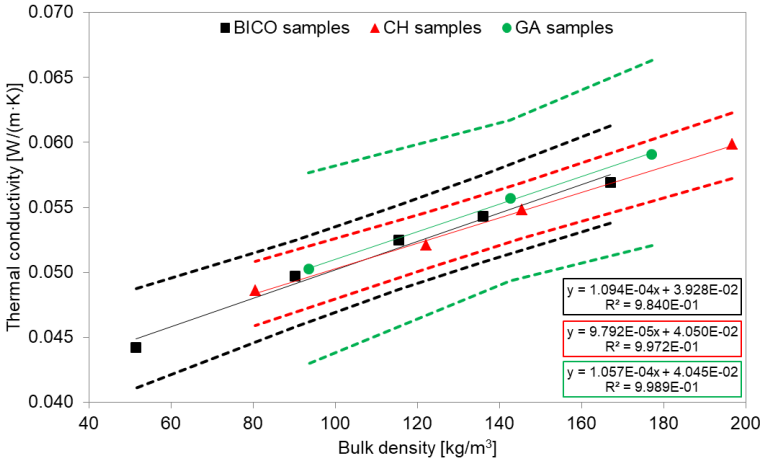

Fig. 8. Thermal conductivity λ vs. bulk density ρ_{bulk} for samples produced using bi-component fibers and chitosan and gum Arabic solution as binder. Dashed curves represent confidence intervals at 95%.

Following the previous analysis, Fig. 8 also shows, in addition to regression lines, the corresponding 95% confidence intervals plotted as the upper and lower dotted lines. These confidence regions were useful in establishing the accuracy of the estimated regression lines. A narrow range of the confidence region was found for BICO and CH samples, while for GA it was quite larger. This was clearly influenced by the greater number of observations n for BICO and CH materials than for GA.

Statistical methods were used to verify whether the rate of change of λ was the same when data sets of different materials were compared. As a first approximation, a comparison between CH and GA samples suggested a thermal conductivity of CH samples about 7% lower than that of the same-density GA samples (Rubino et al., 2019b). The slopes of the regression lines estimated for CH and GA samples were then compared and the null hypothesis $\beta_{CH} = \beta_{GA}$ was verified applying the Student t-test, with $\alpha = 0.05$ (Ortiz et al., 2009). The statistic t_{calc} absolute value was 1.36 and resulted to be less than the critical one $t_{\alpha/2,(n_{CH}+n_{GA}-4)} = 4.18$. Thus, the null hypothesis was accepted at significance level α and the slope β_{CH} and β_{GA} were considered comparable, meaning that in statistical terms the two slopes should be considered the same.

Assuming $\beta_{CH} = \beta_{GA}$, the CH samples were chosen to compare the materials prepared using Co-PET/PET fiber as binder and those produced using bio-binders. The null hypothesis $\beta_{CH} = \beta_{BICO}$ was tested at significance level $\alpha = 0.05$. Being $t_{calc} = 1.20$ lower than $t_{\alpha/2,(n_{CH}+n_{BICO}-4)} = 3.16$, even in this case the null hypothesis was accepted and the slopes of the regression lines of BICO, CH and GA samples were considered comparable. As a

consequence of comparable β parameters, the changes in the bulk densities of the three types of materials affected thermal conductivity values in the same way, regardless of the different fabrication techniques.

The result of the statistical tests could be expected due to the similar porosity values shown by the compared materials. As will be better explained in Section 5.3, the molding process and the chemical binding technique used to interlock together the wool fibers, produced several groups of samples with a void fraction close to 90%. A fibrous material can be considered as a two-component system, i.e. solid and gas medium, and its thermal conductivity is the result of the heat transfer through these two phases (Gong et al., 2014). The air entrapped within the pores affects the thermal behaviour of a fibrous material more than the fibrous matrix, because of its thermal conductivity coefficient with an order of magnitude lower than that of the solid matrix. Thus, being the porosity value exhibited by the same-density BICO, CH, and GA samples close to 0.9, the three materials showed comparable λ values and similar rate of variation.

The properties which characterize the hygric behaviour of the BICO, CH and GA nonwovens are shown in Table 4.

Table 4. Hygric properties of tested BICO, CH and GA materials by varying their density values ρ_{bulk}: mean values of water vapour permeability δ and water vapour resistance factor μ expressed with the standard deviation of the mean.

Tested materials	ρ_{bulk} [kg/m^3]	$\delta \cdot 10^{-11}$ [kg/(m·s·Pa)]	μ [-]
BICO-1	167±6	1.90±0.08	10.3±0.4
BICO-2	136±1	2.15±0.68	9.1±2.9
BICO-3	115±1	2.20±0.27	8.9±1.1
BICO-4	90±2	2.00±0.53	9.8±2.6
BICO-5	51±1	2.20±0.17	8.9±0.7
CH-1	197±2	2.67±0.26	7.4±0.7
CH-2	145±2	2.32±0.33	8.5±1.2
CH-3	122±1	2.56±0.23	7.8±0.7
CH-4	80±1	2.44±0.08	8.0±0.3
GA-1	177±3	2.32±0.12	8.5±0.4
GA-2	143±2	2.27±0.16	8.6±0.6
GA-3	93±1	2.52±0.26	7.8±0.8

The water vapour permeability δ and the water vapour resistance factor μ are given as mean values of experimental results together with measurement uncertainty expressed as the

standard deviation of the mean value (GUM, 2008). The hygric results were compared with those obtained for construction materials characterized by similar density values. The BICO samples showed μ coefficients in agreement with sustainable insulators based on natural materials as wood (μ=9.06, ρ_{bulk}=117 kg/m^3) or cork (μ=5÷10, ρ_{bulk}=100÷220 kg/m^3) (Cetiner et al., 2018, Pfundstein, 2008) and with felts produced from mineral rocks (μ=12, ρ_{bulk}=40÷150 kg/m^3) (UNI 10351, 2015).

In Fig. 9, the distribution of the water vapour permeability values as a function of the bulk density for BICO samples is compared with that for CH and GA samples. For the three types of materials the coefficient of determination R^2, less than 0.7 for each sample, showed a non-significant linear correlation existing between the independent variable ρ_{bulk} and the dependent variable δ. Similar result was further proved by applying a hypothesis test to compare the slope parameter β of the three regression lines. Particularly, the Student's t-test (Ortiz et al., 2009) was performed to verify the null hypothesis $\beta = 0$ at significance level $\alpha = 0.05$. The statistic t_{calc} absolute values computed for BICO, CH and GA samples were respectively 2.14, 0.84 and 1.46; whereas the associated $t_{\alpha/2,(n-2)}$ values were respectively 4.18, 6.21 and 25.45. The $|t_{calc}|$ values resulted to be less than $t_{\alpha/2,(n-2)}$ ones; thus the null hypothesis was rejected in support of the alternative one $\beta \neq 0$. Consequently, no statistically significant relationship was found between ρ_{bulk} and δ whatever the material considered and, in any case, the relations were substantially the same for each subset of values.

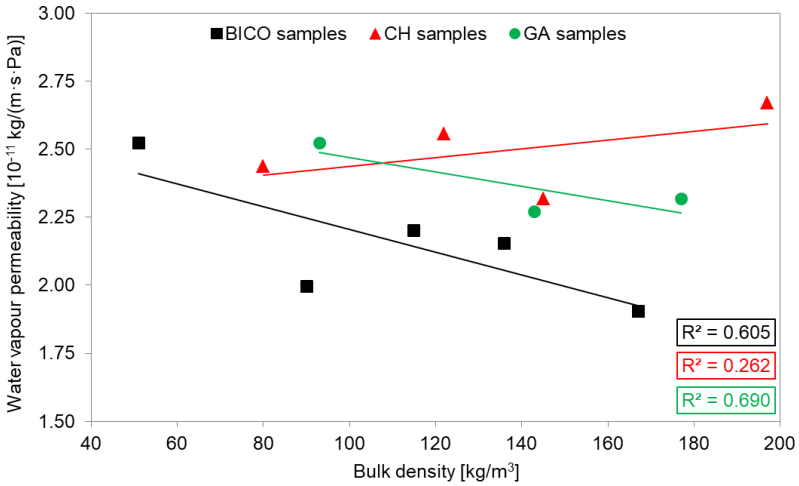

Fig. 9. Water vapour permeability δ vs. bulk density ρ_{bulk} for samples produced using bi-component fibers, chitosan and gum Arabic solution as binder. The solid lines represent the regression lines.

Therefore, in order to better investigate the hygric behaviour of BICO samples and to compare it with that of CH and GA ones, the mean values of the distribution of the three data sets δ were compared. Assuming $\overline{\delta_{BICO}}$, $\overline{\delta_{CH}}$ and $\overline{\delta_{GA}}$ as the average values of the δ data sets of BICO, CH and GA samples, a two samples Student's t-test (Andrade and Estévez-Pérez, 2014) was applied to study whether the difference among the three values could be statistically zero. First, the null hypothesis $\overline{\delta_{CH}} - \overline{\delta_{GA}} = 0$ was tested at significance level $\alpha = 0.05$. Since $|t_{calc}| = 1.13$ was less than $t_{\alpha/2,(n_{CH}+n_{GA}-2)} = 3.16$, the null hypothesis was accepted and the magnitude of the difference between the two mean values was assumed statistically insignificant. As a consequence, CH and GA samples were considered belonging to the same group of materials characterized by a mean water vapour permeability value $\overline{\delta_{CH+GA}} = 2.44 \times 10^{-11}$ kg/(m · s · Pa). Finally, the null hypothesis $\overline{\delta_{CH+GA}} - \overline{\delta_{BICO}} = 0$ was tested at significance level $\alpha = 0.05$. Being $|t_{calc}| = 2.68$ greater than $t_{\alpha/2,(n_{CH+GA}+n_{BICO}-2)} = 2.63$, the null hypothesis was rejected, although the difference between the *t* values was marginal. Therefore, the two means $\overline{\delta_{CH+GA}} = 2.44 \times 10^{-11}$kg/(m · s · Pa) and $\overline{\delta_{BICO}} = 2.16 \times 10^{-11}$kg/(m · s · Pa) were assumed as different, concluding that the samples with bicomponent fibers and natural solutions as binder belong to different groups of materials, although by a statistically marginal amount. The difference between the two mean values $\bar{\delta}$ was a consequence of the effects of the thermal and chemical manufacturing process on the tortuosity values of the final products. In fact, the geometry of the pores plays an important role in describing the water vapour transfer in fibrous building materials (Collet et al, 2011). As will be widely discussed in the next Section 5.3, the BICO samples showed higher tortuosity values than the CH and GA ones, allowing a more complex vapour flow path and consequently a lower water vapour permeability.

A box plot (Fig. 10) was used to provide a visual summary of the distribution of δ data sets of the two groups of materials; i.e. nonwovens obtained using Co-PET/PET fiber as binder and nonwovens prepared with chitosan and gum Arabic binding solutions. As it can be observed, the distribution of the observations belonging to the two sub-sets presents a certain overlapping. However, according to statistical tests mean values can be nonetheless considered as independent.

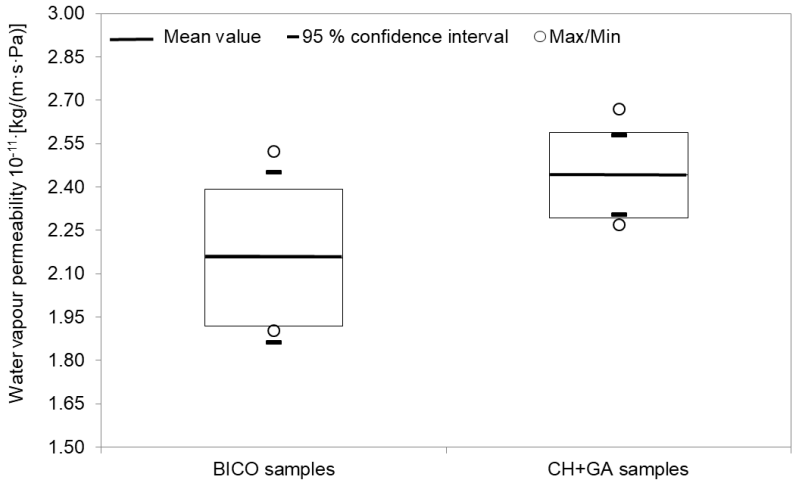

Fig. 10. Box plot of water vapour permeability data sets of BICO, CH and GA samples. Bold line corresponds to mean value, boxes correspond to standard deviations, whiskers to 95% confidence intervals and dots represent the maximum and minimum values.

5.3 Non-acoustic properties

As anticipated in Section 3.5, although the non-acoustic parameters of BICO samples were experimentally measured, the inverse method was also used to estimate them. Table 5 outlines the non-acoustic properties resulting from the measurements and the inverse acoustic characterization; the latter are marked with a star. The mean values of porosity, tortuosity and air flow resistivity are reported together with their measurement uncertainty expressed as the standard deviation of the mean (GUM, 2008).

Table 5. Non-acoustic properties of BICO samples resulting from the experimental measurements: mean values of porosity ε, tortuosity τ and air flow resistivity σ expressed with the standard deviation of the mean. The values of Λ/Λ'*, s* and σ* respectively represent the characteristic length ratio, the shape factor and the flow resistivity determined with the inverse method.

Tested materials	BICO-1	BICO-2	BICO-3	BICO-4	BICO-5
ρ_{bulk} [kg/m^3]	167±6	136±1	115±1	90±2	51±1
ε [-]	0.88±0.0005	0.90±0.0006	0.91±0.0003	0.93±0.0004	0.95±0.0008
τ [-]	2.55±1.17	1.82±0.81	2.16±0.37	1.09±0.11	1.32±0.66
σ [kN·s/m^4]	76.8±16.8	69.4±10.7	59.3±10.5	44.9±12.0	23.6±2.2
σ* [kN·s/m^4]	86.0	54.1	48.6	33.2	23.4
s* [-]	1.35	1.32	1.95	1.40	1.50
Λ/Λ'* [-]	1.00	1.00	1.00	1.00	1.20

The characteristic physical parameters determined only with the inverse method (i.e. the characteristic lengths ratio Λ/Λ' and the shape factor s) are also shown.

The measured porosity values ε varied in the 0.88-0.96 range (depending on the sample), proving the open structure observed by SEM (Fig. 6). These results were similar to those observed for CH and GA samples which showed a porosity varying respectively from 0.86 to 0.94 and from 0.87 to 0.93.

With reference to tortuosity, most theoretical formulations (Matyka et al., 2008; Koponen et al., 1997) express the τ value as a function of the porosity only, even though the tortuosity of a porous media depends on the shape of the pores and their interaction, in addition to the voids volume fraction (Pisani, 2011). Although samples under test should have a tortuosity value close to the unity complying with the idea of a fibrous structure (Willie and Spangles, 1952), some significant difference could be observed among their measured tortuosity values. In fact, Table 5 showed that the tortuosity values τ directly measured for BICO samples varied from 1.09 to 2.55. Conversely, CH samples were characterized by τ values slightly higher than one (τ varied from 1.11 to 1.23). Such results suggested that the different process used to produce the materials could largely affect the geometric complexity of their fibrous microstructure. Likely, when the wool batting was soaked in the chitosan solution and then squeezed, the air trapped in the voids was eliminated and the fibers tended to align. Therefore, samples with a network of pores interconnected following a preferential direction were obtained. Conversely, the richly entangled microstructure resulting from wool carding was better preserved when bi-component fibers were hot molded.

As it can be observed in Table 5, the percent difference between σ and σ^* values varied from about 1% for sample BICO-5 to 26% for sample BICO-4. In Fig. 11, the measured and the "inverse" air flow resistivity values of BICO samples resulted higher than the σ values measured for CH and GA samples. Such result could be explained by the tortuosity measurements. In fact, higher tortuosity values measured for BICO samples implied more intricate flow paths, resulting in less air permeability.

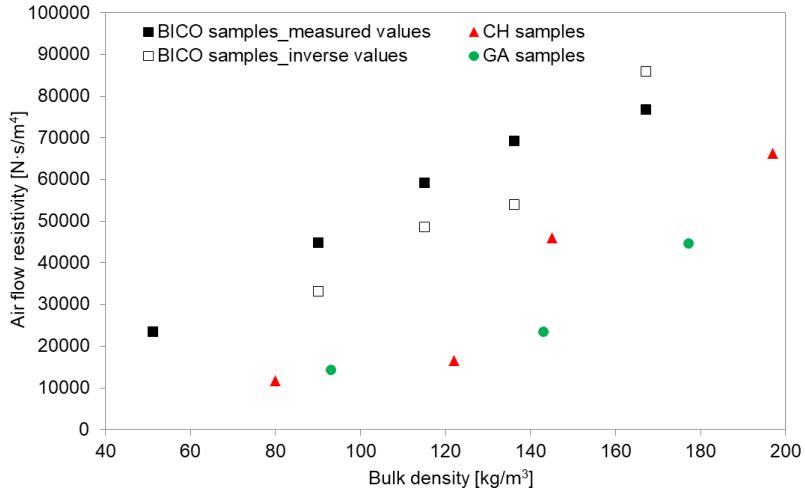

Fig. 11. Air flow resistivity σ vs. bulk density ρ_{bulk} for BICO, CH and GA samples.

The experimental results obtained for non-acoustic properties of the BICO samples were in agreement with those of building materials with similar density values although with completely different structure. Mati-Baouche et al. (2016) showed that sustainable composites produced from sunflowers stalks bonded with chitosan had a bulk density of 186 kg/m^3, a porosity of 0.86, and a tortuosity of about two, similar to investigated fibrous nonwovens. Additionally, a comparable air flow resistivity value of 41.8 kN·s/m^4 was observed.

5.4 Acoustic properties

Fig. 12 plots the mean sound absorption coefficients values resulting from the impedance tube measurements for BICO nonwovens. As it can be seen, the acoustic behaviour of the samples changed according to their air flow resistivity values, providing sound absorption curves with different trends. The BICO-1 sample, having σ^* = 86.0 kN·s/m^4, exhibited a sound absorption curve without evident peaks due to its high air flow resistivity value which reflected the low air permeability of the material. Conversely, the sample BICO-5 showed a σ^* = 23.4 kN·s/m^4, proving to be more permeable to air and showing a sound absorption curve with a peak moving towards medium and high frequencies, while its absorption in the low frequency range became weaker than BICO-1. The remaining samples, characterized by σ^* value between 86.0 and 23.4 kN·s/m^4, showed intermediate acoustic behaviours between that of BICO-1 and BICO-5 samples.

The BICO-4 sample, having σ^* = 33.2 kN·s/m^4, exhibited a behaviour similar to that of BICO-5, with sound absorption coefficients which sharply increased at medium and high frequencies. However, some differences in the location of the first peak of the two materials

could be noticed. For BICO-4, the first peak appeared at 1000 Hz, with α rising up to almost 0.9; while for sample BICO-5 the first peak appeared at 1250 Hz, with α rising up to almost the unity.

At the same frequencies, lower sound absorption properties were observed for the samples BICO-2 and BICO-3 which exhibited α coefficients almost overlapped at all frequencies as a consequence of their comparable σ* values (i.e. 54.1 kN·s/m^4 for BICO-2 and 48.6 kN·s/m^4 for BICO-3). For both samples, α was equal to about 0.8 at 1000 Hz and just over 0.8 at 1250 Hz. The sound absorption coefficients trend of the samples BICO-2 and BICO-3 could be considered similar to that of BICO-1 sample due to their sound absorption curves shifted towards low frequencies, with α values higher than BICO-4 and BICO-5 samples up to 400 Hz. However, starting from 500 Hz, the sound absorption coefficients of the BICO-2 and BICO-3 samples were about 0.1 higher than BICO-1 sample, without showing evident peaks.

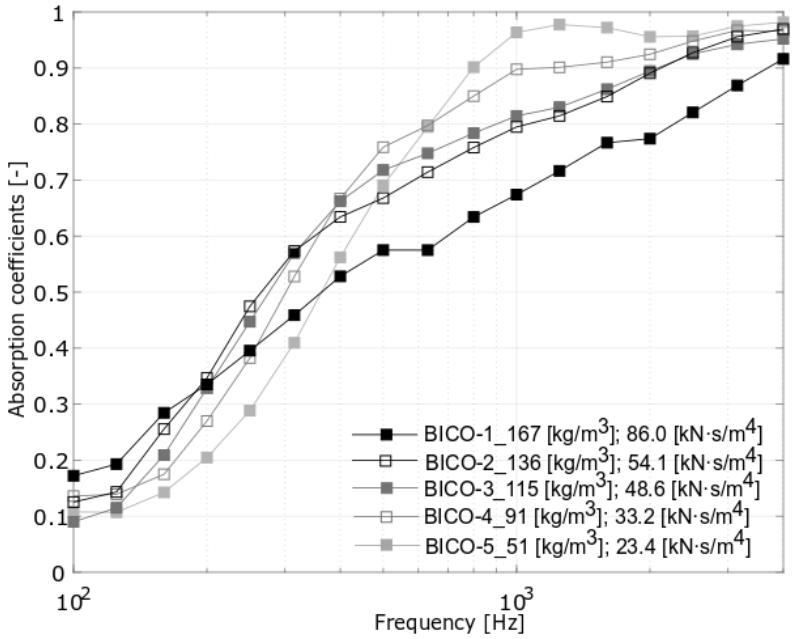

Fig. 12. Mean measured normal incidence sound absorption coefficients of BICO samples.

The acoustic behaviour of the investigated BICO samples was then discussed by comparing the sound absorption curve resulting from the impedance tube measurements with values predicted by Delany-Bazley and Johnson–Champoux–Allard theoretical models.

Following the previously described determination of the non-acoustic parameters according to both direct measurement and inverse method, the subsequent discussion was referred to predictions based on the “optimized” parameters and, for comparison purposes, on the measured values of flow resistivity which is the only parameter used by D&B model. The

absolute error expressed as a mean value of the absolute difference between the sound absorption coefficients predicted by the theoretical models and those resulting from the experimental measurements was used to test the accuracy of the predicted sound absorption curves.

As previously mentioned in Section 3.5, JCA models was fed using the directly measured values of porosity ε and tortuosity τ; while the values of the characteristic physical properties (Λ/Λ'* and s*) and the air flow resistivity σ* were estimated by the inverse algorithm.
Taking into account the D&B model, the "inverse" value of the air flow resistivity was used.

Table 6 shows the mean absolute errors ($e_{D\&B}$ and e_{JCA}) of the sound absorption coefficients when the measured air flow resistivity values were used to fed the JCA and D&B models and the mean absolute errors ($e_{D\&B}$* and e_{JCA}*) obtained using the estimated air flow resistivity values. As it can be observed, the use of optimization techniques allowed to significantly reduce the error values $e_{D\&B}$ and e_{JCA}.

Table 6. The mean absolute errors $e_{D\&B}$ and e_{JCA} of the sound absorption coefficients when the measured air flow resistivity values are used to fed the JCA and D&B models and the mean absolute errors $e_{D\&B}$* and e_{JCA}* obtained using the estimated air flow resistivity values in the JCA and D&B.

Tested materials	$e_{D\&B}$ [-]	$e_{D\&B}$* [-]	e_{JCA} [-]	e_{JCA}* [-]
BICO-1	0.0345	0.0475	0.0297	0.0186
BICO-2	0.0870	0.0564	0.0494	0.0273
BICO-3	0.0686	0.0468	0.0480	0.0292
BICO-4	0.0600	0.0464	0.0465	0.0267
BICO-5	0.0323	0.0325	0.0161	0.0159

Fig. 13a compares measured and predicted sound absorption coefficients of BICO-1 samples. The comparison with the theoretical curves pointed out that the D&B empirical model gave rise to significant discrepancies, despite the σ* value was used to implement the model. On the contrary, the JCA model almost perfectly predicted the trend of the experimental absorption coefficients of the sample.

A similar result was observed when the experimental and the theoretical sound absorption curves of the samples BICO-2 and BICO-3 were compared (Fig. 13b). The JCA model predicted the measured values of the two materials better than the D&B one. Although significant discrepancies appeared from 250 Hz to 400 Hz, the phenomenological model allowed a rather precise estimation of the absorption coefficients fluctuations starting from 800 Hz.

Fig. 13c plots the acoustic behaviours of the samples BICO-4 and BICO-5. It can be noted that the phenomenological approach allowed a rather good estimation of first peak location, its maximum-minimum fluctuations and values of absorption coefficients for both materials. However, slightly larger discrepancies between measurements and predictions could be appreciated for BICO-4 sample in the medium frequencies range from 250 to 500 Hz, where the JCA model slightly underestimated the measured absorption coefficients. D&B model predicted the acoustic behaviour of both BICO-4 and BICO-5 samples better than of the remaining three materials. Possibly, this occurs because BICO-4 and BICO-5 were the only samples having air flow resistivity lower than 50 kN·s/m^4, which is the upper limit for a safe application of the empirical model.

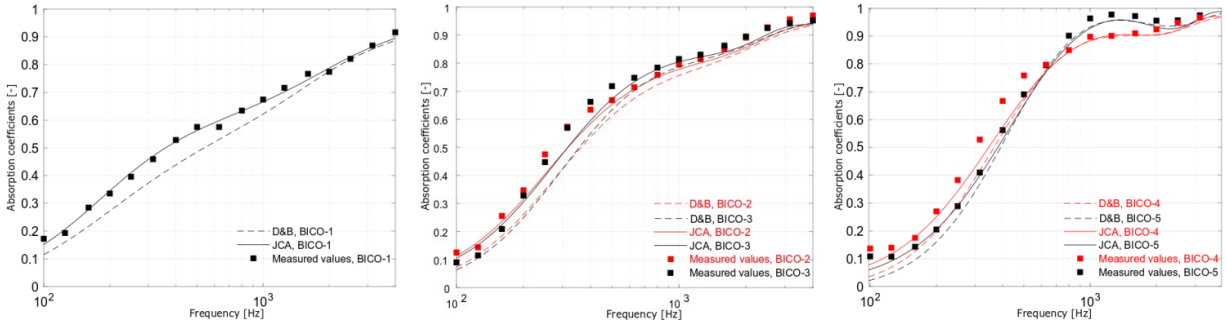

(a) (b) (c)

Fig. 13. Comparison between mean measured normal incidence sound absorption coefficients and those predicted by the D&B and JCA model for BICO-1 sample (a), BICO-2 and BICO-3 samples (b) and BICO-4 and BICO-5 samples (c)

Finally, measured sound absorption curves of BICO samples were compared with those measured for CH and GA samples, in order to provide a complete analysis of the possible effects of the manufacturing processes on the sound absorption behaviour of the fibrous materials (Fig. 14). Samples having similar air flow resistivity values were compared. Thus, BICO-1 and BICO-4 samples were not taken into account in the comparison because of their air flow resistivity largely different from those characterizing the CH and GA samples.

In Fig. 14a, BICO-2 and CH-1 samples are compared. Although the ρ_{bulk} value of BICO-2 sample was about 31% lower than that of CH-1, the two materials showed comparable air flow resistivity values, differing by about 15%. Similar air flow resistivity properties could be explained due to the tortuosity value measured for BICO-2 material which was higher than that measured for CH-1 (τ was 1.82 for BICO-2 materials and 1.23 for CH-1). The high τ value resulted in a more intricate microscopic air flow paths for the BICO-2 sample than CH-

1, allowing to obtain materials with similar air flow resistivity values, regardless of their different bulk densities.

In Fig. 14b, BICO-3 sample is compared with CH-2 and GA-1 ones. The BICO-3 material showed an air flow resistivity value about of 5% lower than CH-2, while being 21% lighter. This could be explained, again, because of the tortuosity value which was 2.16 for BICO-3 sample and 1.11 for CH-2 sample. The high τ value increased the air flow permeability of BICO-3 sample, allowing to obtain a material with the same sound absorption behaviour of CH-2 one, although a lower bulk density value.

Similar considerations could be made for the analysis of BICO-3 and GA-1 samples, but no direct measure of tortuosity was available for GA samples. Nonetheless, BICO-3 sample showed an air flow resistivity value about 8% higher than GA-1 sample, although its density value was about 35% lower.

Fig. 14c displays the sound absorption curves measured for BICO-5 and GA-2 samples, having air flow resistivity values differing by only 2% and bulk density values differing by 64%. As it can be seen, BICO-4 and GA-2 materials showed measured sound absorption curves almost perfectly overlapping up to 630 Hz. At 1250 Hz, the first peak of BICO-5 sample appeared with α raising up to almost the unity, whereas the GA-2 sample showed an α value of 0.9, likely because of the higher density.

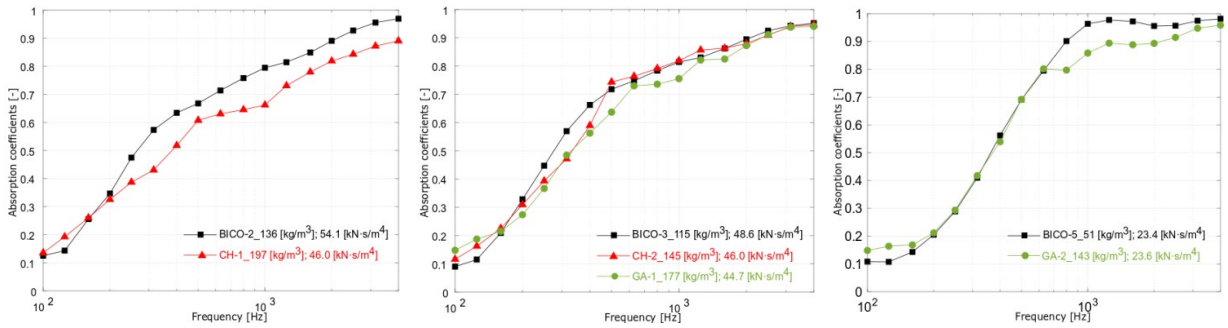

(a) (b) (c)

Fig. 14. Comparison between mean normal incidence sound absorption coefficients measured for BICO-2 and CH-1samples (a), BICO-3, CH-2 and GA-1 samples (b) and BICO-5 and GA-2 samples (c)

6. Discussion and limitations

Based on the achieved experimental thermal results, all the investigated materials could be considered a good solution to limit the heat exchange between outdoors and indoors of buildings, providing a suitable internal comfort and reducing the energy consumption and emissions associated to HVAC systems. Comparison with commercially available products and other experimental materials investigated in other researches proved that performances are perfectly in line and, in some cases, even better. Consequently, the investigated materials had a high potential as non-structural panels for thermal insulation and sound absorption of internal and external walls in civil and industrial applications.

Among the possible restrictions in the use of the proposed sustainable panels, even though mechanical properties will be better investigated in subsequent researches, it is easily predictable that low density panels might not be self-bearing and should be carefully handled, being preferably used to fill air gaps. In general, wool is known for its ability to absorb and release water vapor, but direct contact with liquid water should be avoided. In fact, although wool is impermeable to small amounts of water, its thermal performance could be negatively affected. The durability of materials (i.e. the presence of toxic species into the building components) is also an important issue for assessing their performance and, consequently, the quality of a building (Bennacer et al., 2016). Fungi and moulds could decay the performances of building materials and affect indoor air quality. Although at this stage of our research the antimicrobial behaviour of the investigated materials was not directly studied, literature researches provides convincing arguments in favor of their durability. In fact, wool fibers represent a suitable raw material to avoid the attack by biological agents such as mildew (Tridico, 2009). The wool-polyester combination supports the antimicrobial behaviour of the building components by the inherent resistance of synthetic fibers to micro-organism proliferation. Trajković et al. (2016) observed that no ageing and no loss of mass took place on polyester waste materials. With reference to chemically bonded samples, Elinwa (2018) and Mohamed et al., (2020) confirmed the capacity of gum Arabic to improve physical and mechanical properties of the cement binders and the improvement of the durability and the resistance to the acid attack. Ahmed (2018) demonstrated that the antibacterial property of tannins in the gum Arabic plant. Also the chitosan has been revived due to its antimicrobial action (Bakshi et al. 2020, Vinod et al. 2020) in different application fields (i.e. food, medical, textile, agriculture).

Another issue that might raise some concerns is the end-of-life behavior of the proposed samples. Although the disposal of samples made with bi-component fibers as binders may seem more problematic than that of the samples made with sustainable solutions of chitosan and gum Arabic, the treatment of mixed fibers is not a new issue. Nowadays, the most part of fabrics are blends of synthetic and natural fibers. The presence of non-biodegradable synthetic materials makes the decomposition of natural fibers more difficult, favoring the landfilled or the incineration of the textile waste (Pensupa, 2020). However, the possible reuse of textile waste made of mixed fibers to produce industrial wipes or filling materials may represent a significant advantage in terms of use of virgin materials and environmental impact, even if compared to incineration (Schmidt et al.2016). Obviously, to make the recovery of textile waste really effective, it would be necessary to recycle the fibers separately (Östlund et al., 2017). From this point of view Yousef et al. (2020), tested an ecofriendly hydrophilicity solvent to separate polyester from cotton in jeans fabrics, proving a significant reduction of 1448 kg CO_2 equivalents per ton of waste than usual approaches (i.e. landfilled and incineration). A similar recycling technique could be applicable to solve the end-of-life issue of all products made with different types of fibers, even if they do not find direct application in the textile field.

7. Conclusions

The present paper investigated the possibility to reprocess 100% wool cutoffs in secondary raw materials for the production of building nonwovens, using polyester/copolyester bi-component fibers as binder. Building panels with different density values were analyzed from different perspectives and their hygric, thermal and acoustic behaviours were compared with those of composite materials produced using similar raw materials, but chitosan and gum Arabic solutions as binders. The main findings were:

- statistical analysis proved that changes in the bulk densities of the three different types of materials affected in the same way their thermal conductivity values. On the contrary, the technique followed to produce the nonwoven (with or without binders) affected pore microstructure with consequent implications on the sound absorption and water vapour diffusion properties;
- all the materials exhibited suitable thermal properties (i.e. thermal conductivity less than 0.06 W/(m·K)) to be used as thermal insulation panels;

- all materials, apart from samples with the highest density, showed good sound absorption coefficients as high as 0.7 at frequencies from 500 Hz on;
- the mean values of water vapour permeability resulted to be $2.441 \cdot 10^{-11}\mathrm{kg}/(\mathrm{m} \cdot \mathrm{s} \cdot \mathrm{Pa})$ for samples produced using natural solutions as binder agents, and $2.155 \cdot 10^{-11}\mathrm{kg}/(\mathrm{m} \cdot \mathrm{s} \cdot \mathrm{Pa})$ for samples using bi-component binder fibers; the two values were in agreement with the current construction standards.

In the light of the above mentioned results, the proposed materials might be conveniently used to fill air gaps in masonry walls, or as internal finishing (including also acoustic benefits).

From an environmental point of view, the reprocessing of textile cutoffs in secondary raw materials allowed to divert waste from landfills and incineration, reducing the use of virgin resources. However, further investigations are under way in order to define the environmental and the economic effects of the two different nonwoven techniques. Furthermore, a life cycle assessment of the three types of binding agents used (i.e. chitosan and gum Arabic solutions and bicomponent fibers) is under way to better clarify which solution is more eco-friendly.

References

Ahmed, A.A., 2018. Health benefits of gum arabic and medical use, in: Mariod A.A. (Ed), Gum Arabic_Structure, Properties, Application and Economics. Academic press, United Kingdom, pp183-210.

Allard, J.F., Champoux, Y., 1992. New empirical equation for sound propagation in rigid frame fibrous material. J. Acoust. Soc. Am. 91, 3346-3353. https://doi.org/10.1121/1.402824.

Anand, S.C., Swarbrick, G., Russell, S.J., 2006. Mechanical bonding, in: Russell, S.J. (Ed), Handbook of nonwovens. Woodhead Publishing, England, pp. 201-297.

Andrade, J.M. and Estévez-Pérez, M.G., 2014. Statistical comparison of the slopes of two regression lines: A tutorial. Anal. Chim. Acta 838, 1-12. http://dx.doi.org/10.1016/j.aca.2014.04.057.

Atalla, Y. and Panneton, R., 2005. Inverse acoustical characterization of open cell porous media using impedance tube measurements. Can. Acoust. 33(1), 11-24. //jcaa.caa-aca.ca/index.php/jcaa/article/view/1711.

Avcioglu Kalebek, N. and Babaarslan, O., 2016. Fiber selection for the production of nonwovens, in: Jeon, H.-Y. (Ed), Non-woven fabrics. IntechOpen, pp. 1-32.

Baccouch, W., Ghith, A., Yalcin-Enis, Y., Sezgin, H., Miled, W., Legrand, X., Faten, F., 2020. Investigation of the mechanical, thermal, and acoustical behaviors of cotton, polyester, and cotton/polyester nonwoven wastes reinforced epoxy composites. J. Ind. Text. 0, 1-24. https://doi.org/10.1177/1528083720901864.

Balador, Z., Gjerde, M., Isaacs, N., 2020. Influential factors on using reclaimed and recycled building materials, in: Littlewood, J., Howlett, R., Capozzoli, A., Jain, L. (Eds), Sustainability in Energy and Buildings, 163. Springer, Singapore, pp. 37-47.

Bakatovich, A., Gaspar, F., 2019. Composite material for thermal insulation based on moss raw material. Constr. Build. Mater., 228, 116699. https://doi.org/10.1016/j.conbuildmat.2019.116699.

Bakshi, P.S., Selvakumar, D., Kadirvelu, K., Kumar, N.,S., 2020. Chitosan as an environment friendly biomaterial – a review on recent modifications and applications. Int. J. Biol. Macromol., 150, 1072-1083. https://doi.org/10.1016/j.ijbiomac.2019.10.113.

Bear, J., 1988. Dynamics of Fluids in Porous Media. American Elsevier Publishing Co, New York.

Bennacer, R., Abahri, K., Belarbi, R., 2016. Intrinsic properties controlling the sustainability of construction in: Khatib, M.J. (Ed), Sustainability of construction materials. Woodhead publishing series in civil and structural engineering: number 70, United Kingdom, pp. 33-54.

Bilal, M., Ahmad Khan, K.I., Thaheem, M. J., Nasir, A.R., 2020. Current state and barriers to the circular economy in the building sector: towards a mitigation framework. J. Clean. Prod. In press. https://doi.org/10.1016/j.jclepro.2020.123250.

Bozaci, E., Arik, B., Demir, A., Özdoğan, E., 2012. Potential use of new methods for identification of hollow polyester fibers. Tekstil ve Konfeksiyon, 22, (4), 317-323. (nel testo è erroneamente riportato con il riferimento Özdoğan…me lo sono segnato e lo correggerò nella versione definitiva)

Brown, R.J.S., 1980. Connection between formation factor for electrical resistivity and fluid-solid coupling factors in Biot's equations for acoustic waves in fluid-filled porous media. Geophysics 45(8), 1269-1275. https://doi.org/10.1190/1.1441123.

Brydon, A.G. and Pourmohammadi, A., 2006. Dry-laid web formation, in: Russell, S.J. (Ed), Handbook of nonwovens. Woodhead Publishing, England, pp. 16-111.

Çelikel, D.C. and Babaarslan, O., 2017. Effect of bicomponent fibers on sound absorption properties of multilayer nonwovens. J. Eng. Fiber. Fabr. 12(4), 15-25. https://doi.org/10.1177/155892501701200403.

Cerkez, I., Kocer, H. B., Broughton, R. M., 2017. Airlaid nonwoven panels for use as structural thermal insulation. J. Text. Inst.109 (1), 1-7. https://doi.org/10.1080/00405000.2017.1320815.

Cetiner, I. and Shea, A.D., 2018. Wood waste as an alternative thermal insulation for buildings. Energ. Buildings 168, 374–384. https://doi.org/10.1016/j.enbuild.2018.03.019.

Circular economy package. Four legislative proposals on waste. Briefing EU Legislation in Progress July 2018. Available at: https://www.europarl.europa.eu/RegData/etudes/BRIE/2018/625108/EPRS_BRI(2018)625108_EN.pdf (Accessed April 2020).

Collet F., Achchaq F., Djellab K., Marmoret L., Beji H., 2011. Water vapor properties of two hemp wools manufactured with different treatments. Constr. Build. Mater., 25, 1079-1085. https://doi.org/ 10.1016/j.conbuildmat.2010.06.069.

Cox, T.J. and D'Antonio, P.K., 2004. Acoustic Absorbers and Diffusers, Theory, Design and Application, Spon Press, London, pp. 141-145.

Danihelová, A., Nemec, M., Gergel', T., Gejdoš, M., Gordanová J., Sˇcensný, P., 2019. Usage of recycled technical textiles as thermal insulation and an acoustic absorber. Sustainability 11 (10), 2968. https://doi.org/10.3390/su11102968.

Delany, M.E. and Bazley, E.N., 1970. Acoustical properties of fibrous materials. Appl. Acoust. 3 (2), 105-116. https://doi.org/10.1016/0003-682X(70)90031-9.

Drochytka, R., Dvorakova, M., Hodna, J., 2017. Performance evaluation and research of alternative thermal insulation based on waste polyester fibers. Procedia Eng. 195, 236-243. https://doi.org/10.1016/j.proeng.2017.04.549.

Elinwa, A., U., Abdulbasir G., Abdulkadir G., 2018. Gum Arabic as an admixture for cement concrete production. Constr. Build. Mater., 176, 201-212. https://doi.org/10.1016/j.conbuildmat.2018.04.160.

El Wazna, M., Gounni, A., El Bouari, A., El Alami, M., Cherkaoui, O., 2019. Development, characterization and thermal performance of insulating nonwoven fabrics made from textile waste. J. Ind. Text. 48 (7), 1-17. https://doi.org/10.1177/1528083718757526.

EN 12086, 2013. Thermal insulating products for building applications Determination of long term water absorption by diffusion. http://store.uni.com/catalogo/uni-en-12088-2013 (Accessed April 2020).

Forouharshad, M., Montazer, M., Moghadam, M.B., Saligheh, O., 2011. Preparation of flame retardant wool using zirconium acetate optimized by CCD. Thermochim. Acta 520 (1-2), 134-138. https://doi.org/10.1016/j.tca.2011.03.029.

Gong, L., Wang, Y., Cheng, X., Zhang, R., Zhang, H., 2014.A novel effective medium theory for modeling the thermal conductivity of porous materials. Int. J. Heat. Mass. Transf. 68, 295-298. https://doi.org/10.1016/j.ijheatmasstransfer.2013.09.043.

Gowane, G.R., Gadekar, Y.P., Prakash, V., Kadam V., Chopra, A., Prince L.L.L., 2017. Climate change impact on sheep production: growth, milk, wool, and meat, in: Sejian V., Bhatta R., Gaughan J., Malik P., Naqvi S., Lal R. (Eds), Sheep production adapting to climate change, Springer, Singapore, pp.31-69.

Hittini, W., I. Mourad, A.-H., Abu-Jdayil, B., 2019. Cleaner production of thermal insulation boards utilizing buffing dust waste. J. Clean. Prod. 236, 117603. https://doi.org/10.1016/j.jclepro.2019.117603.

Ingard, U.K. and Dear, T.A., 1985. Measurement of acoustic flow resistance. J. Sound Vib., 103(4), 567-572. https://doi.org/10.1016/S0022-460X(85)80024-9.

Islam, S., Bhat, G., 2019. Environmentally-friendly thermal and acoustic insulation materials from recycled textiles. J. Environ. Manage. 251, 109536. https://doi.org/10.1016/j.jenvman.2019.109536.

ISO 11357-1, 2016. Plastics Differential Scanning Calorimetry (DSC) Part 1: general principles. https://www.iso.org/standard/70024.html (Accessed April 2020).

ISO 10534-2, 1998. Acoustics – Determination of sound absorption coefficient and impedance in impedance tubes – Part 2: transfer-function method. https://www.iso.org/standard/22851.html, (Accessed April 2020).

ISO/IEC Guide 98-3, 2008. Uncertainty of Measurement – Part 3: Guide to the expression of Uncertainty in Measurement (GUM:1995). https://www.iso.org/sites/JCGM/GUM-JCGM100.htm, (Accessed April 2020).

Johnson, D.L., Koplik, J., Dashen, R., 1987. Theory of dynamic permeability and tortuosity in fluid-saturated porous media. J. Fluid Mech. 176, 379-402. https://doi.org/10.1017/S0022112087000727.

Korjenic, A., Zach, J., Jitka, J., 2016. The use of insulating materials based on natural fibers in combination with plant facades in building constructions, Energy Build. 116, 45–58. http://dx.doi.org/10.1016/j.enbuild.2015.12.037.

Khan, A., Mohamed, M., Al Halo, N., Benkreira, H., 2017. Acoustical properties of novel sound absorbers made from recycled granulates. Appl. Acoust. 127, 80-88. https://doi.org/10.1016/j.apacoust.2017.05.035.

Koponen, A., Kataja, M., Timonen, J., 1997. Permeability and effective porosity of porous media. Phys. Rev.E 56, 3319-3325. https://doi.org/10.1103/PhysRevE.56.3319.

Kremensas., A., Stapulionienė., R., Vaitkus., S., Kairytė., A., 2017. Investigations on physical-mechanical properties of effective thermal insulation materials from fibrous hemp. Procedia Eng. 172, 586-594. https://doi.org/10.1016/j.proeng.2017.02.069.

Leal Filho, W., Ellam, D., Han, S., Tyler, D., Boiten, V.J., Paço, A., Moora, H., Balogun, A.-L., 2019. A review of the socio-economic advantages of textile recycling. J. Clean. Prod. 218, 10-20. https://doi.org/10.1016/j.jclepro.2019.01.210.

Lee, Y., Joo, C., 2003. Sound absorption properties of recycled polyester fibrous assembly absorbers. AUTEX Res. J. 3 (2), 78-84. http://www.autexrj.org/No2-2003/0047.p.

Li, W.D. and Ding E.Y., 2007. Preparation and Characterization of Poly(ethylene terephthalate) Fabrics Treated by Blends of Cellulose Nanocrystals and Polyethylene Glycol. J. Appl. Polym., 105, 373-378. https://doi.org/10.1002/app.26098.

Liuzzi, S., Rubino, C., Martellotta, F., Stefanizzi, P., Casavola, C., Pappalettera, G., 2020. Characterization of biomass-based materials for building applications: The case of straw and olive tree waste. Ind. Crops Prod. 147, 112229. https://doi.org/10.1016/j.indcrop.2020.112229.

Martellotta, F., Cannavale, A., De Matteis, V., Ayr, U., 2018. Sustainable sound absorbers obtained from olive pruning wastes and chitosan binder. Appl. Acoust. 141, 71-78. https://doi.org/10.1016/j.apacoust.2018.06.022.

Mati-Baouche, N., de Baynast, H., Michaud, P., Dupont, T., Leclaire, P.,2016. Sound absorption properties of a sunflower composite made from crushed stem particles and from chitosan bio-binder. Appl. Acoust. 111, 179-187. http://dx.doi.org/10.1016/j.apacoust.2016.04.021.

Matyka, M., Khalili, A., Koza, Z., 2008. Tortuosity–porosity relation in the porous media flow. Phys. Rev. E 78, 026306. https://doi.org/10.1103/PhysRevE.78.026306.

Mochizuki, M. and Matsunaga, N., 2016. Bicomponent Polyester Fibers for Nonwovens, in: The society of fiber science and techno, Japan (Ed), High-performance and specialty fibers: concepts, technology and modern applications of man-made fibers for the future, Springer, Tokyo, pp. 395-408.

Mohamed, A., M., Ariffin, M., A., M., Smaoui, H., Osman, M., H., 2020. Performance evaluation of concrete with Arabic gum biopolymer. Mater. Today, In press. https://doi.org/10.1016/j.matpr.2020.04.576.

Munaro, M.R., Tavares, S.F., Bragança, L., 2020. Towards circular and more sustainable buildings: A systematic literature review on the circular economy in the built environment. J. Clean. Prod. 260, 121134. https://doi.org/10.1016/j.jclepro.2020.121134

Muthu, S.S., Li, Y., Hu, J.Y., Mok, P.-Y., 2012a. Recyclability Potential Index (RPI): The concept and quantification of RPI for textile fibers. Ecological Indicators 18, 58-62. https://doi.org/10.1016/j.ecolind.2011.10.003.

Muthu, S.S., Li, Y., Hu, J.Y., Ze, L., 2012b. Carbon footprint reduction in the textile process chain: recycling of textile materials. Fiber. Polym. 13(8), 1065-1070. https://doi.org/10.1007/s12221-012-1065-0.

Muthukumar, N., Thilagavathi, G., Neelakrishnan S., Poovaragan, P.T., 2017. Sound and thermal insulation properties of flax/low melt PET needle punched nonwovens. J. Nat. Fibers 16 (2), 245-252. https://doi.org/10.1080/15440478.2017.1414654.

Naeimirad, M., Zadhoush, A., Kotek, R., Neisiany, R.E., Khorasani, S.N., Ramakrishna S., 2018. Recent advances in core/shell bicomponent fibers and nanofibers: A review. J. Appl. Polym. 135 (21), 46265. https://doi.org/10.1002/app.46265.

Nakanishi, E.Y., Cabral, M.R., de Souza Gonçalves, P., dos Santos, V., Junior., H.S., 2018. Formaldehyde-free particleboards using natural latex as the polymeric binder. J. Clean. Prod. 195, 1259-1269. https://doi.org/10.1016/j.jclepro.2018.06.019.

Ortiz, M.C., Sánchez, S., Sarabia, L., 2009. Quality of analytical measurements: univariate regression, in: S.D., Brown, R., Tauler, B., Walczack (Eds.), Comprehensive chemometrics: chemical and biochemical data analysis, vol. 1, Amsterdam, pp. 128-168.

Östlund, A., Syrén, P.O., Jönsson, C., Ribitsch, D., Syrén, M., 2017. Re:Mix–Separation and recycling of textile waste fiber blends, MISTRA Future Fashion report, Rise: Borås, Sweden.

Payne, A., 2015. Open- and closed-loop recycling of textile and apparel products, in: Muthu, S. (Ed.), Handbook of Life Cycle Assessment (LCA) of textiles and clothing. Woodhead Publishing, Cambridge, United Kingdom, pp. 103-123.

Pensupa, N. 2020. Recycling of end-of-life clothes, in: Rajkishore, N., (Ed), Sustainable Technologies for Fashion and Textiles. Woodhead Publishing Series in Textiles, United Kingdom, pp. 251-309.

Pfundstein, M., Gellert, R., Spitzner, H.M., Rudolphi, A., 2008. Properties of insulating materials in: Schulz, C., (Ed), Insulation Materials: Principles, Materials, Applications. Birkhauser, Basel, pp. 8-15.

Pielesz, A., Freeman, H.S., Wesełucha-Birczyńska, A., Wysocki, M., Włochowicz, A., 2003. Assessing secondary structure of a dyed wool fibre by means of FTIR and FTR spectroscopies. J. mol. Struct. 651, 405-418. https://doi.org/10.1016/S0022-2860(03)00210-2.

Pisani, L.,2011. Simple expression for the tortuosity of porous media. Transport Porous Med. 88 (2), 193-203. https://doi.org/10.1007/s11242-011-9734-9.

Pourmohammadi, 2006. Thermal bonding in: Russell, S.J. (Ed), Handbook of nonwovens. Woodhead Publishing, England, pp. 298-329.

Ramamoorthy, S.K., Persson, A., Skrifvars, M., 2014. Reusing textile waste as reinforcements in composites. J. Appl. Polym. Sci. 131 (17), 3-16. https://doi.org/10.1002/app.40687.

Rubino, C., Bonet-Aracil, M., Liuzzi, S., Martellotta, F., Stefanizzi, P., 2019a. Thermal characterization of innovative sustainable building materials from wool textile fibers waste. IJES 63(2-4), 277-283. https://doi.org/10.18280/ti-ijes.632-423.

Rubino, C., Bonet-Aracil, M., Gisbert-Payá J., Liuzzi, S., Zamorano Cantó M., Martellotta, F., Stefanizzi, P., 2019b. Composite eco-friendly sound absorbing materials made of recycled textile waste and biopolymers. Materials 12 (23), 4020. https://doi.org/10.3390/ma12234020.

Sandin, G., Peters, G.M., 2018. Environmental impact of textile reuse and recycling: A review. J. Clean. Prod. 184, 353-365. https://doi.org/10.1016/j.jclepro.2018.02.266.

Sandin, G., Roos, S., Johansson, M., 2019. Environmental Impact of Textile Fibers-What We Know and What We Don't Know, MISTRA Future Fashion report: 03 part 2, Rise AB: Göteborg, Sweden.

Schmidt, A.; Watson, D.; Roos, S.; Askham, C.; Brunn Poulsen, P., 2016. Mixed fibres in: Gaining benefits from discarded textiles. Rosendahls-Schultz Grafisk, Hillerød, Denmark, pp. 112-116.

Stefan de Carvalho, P., Nora M.,D., Cantorski da Rosa, L., Development of an acoustic absorbing material based on sunflower residue following the cleaner production techniques, J. Clean. Prod. In press. https://doi.org/10.1016/j.jclepro.2020.122478.

Trajković, D., Jordeva, S., Tomovska, E., Zafirova, K., 2016. Polyester apparel cutting waste as insulation material. J. Text. Inst. 108 (7), 1238-1245. https://doi.org/10.1080/00405000.2016.1237335.

Tridico, S.R. 2009. Natural animal textile fibers: Structure, characteristics and identification, in: Houck, M.M. (Ed), Identification of Textile Fibers. Woodhead Publishing in Textiles, New York, pp. 27–67.

UNI 10351, 2015. Building materials and products - Hygrothermal properties - Procedure for determining the design values. http://store.uni.com/catalogo/index.php/uni-10351-2015,

Vinod, A., Sanjay, M.,R., Siengchin, S., Parameswaranpillai, J., 2020. Renewable and sustainable biobased materials: An assessment on biofibers, biofilms, biopolymers and biocomposites. J. Clean. Prod. 258, 120978. https://doi.org/10.1016/j.jclepro.2020.120978.

Willie, M.R.J. and Spangles, M.B., 1952. Application of electrical resistivity measurements to problem of fluid flow in porous media. Am. Assoc. Pet. Geol. Bull, 36 (2), 359-403. https://doi.org/10.1306/3D934403-16B1-11D7-8645000102C1865D.

Wilson, A., 2006. Development of the nonwovens industry in: Russell, S.J. (Ed), Handbook of nonwovens. Woodhead Publishing, England, 1-15.

Wojciechowska, E., Rom, M., Włochowicz, A., Wysocki, M., Wesełucha-Birczyńska, A., 2004. The use of Fourier transform-infrared (FTIR) and Raman spectroscopy (FTR) for the investigation of structural changes in wool fibre keratin after enzymatic treatment. J. Mol. Struct., 704 (1-3), 315-321. https://doi.org/10.1016/j.molstruc.2004.03.044.

Wunderlich, B, 1980. Macromolecular physics, volume 3 - crystal melting. Academic press, New York.

Yousef, S., Tatariants, M., Tichonovas, M., Kliucininkas, L., Lukošiūtė, S.I., Yan, L., 2020. Sustainable green technology for recovery of cotton fibers and polyester from textile waste. J. Clean. Prod.254, 120078. https://doi.org/10.1016/j.jclepro.2020.120078.

Zargarkazemi, A., Sadeghi-Kiakhani, M., Arami, M., Bahrami, S.H., 2015. Modification of wool fabric using prepared chitosan-cyanuric chloride hybrid. J Text I 106 (1), 80-89. https://doi.org/10.1080/00405000.2014.906097.

Zhang, W., Yi, X., Sun, X., Zhang, Y., 2008. Surface modification of non-woven poly (ethylene terephthalate) fibrous scaffold for improving cell attachment in animal cell culture. J. Chem. Technol. Biotechnol., 83, 904-911. https://doi.org/10.1002/jctb.1890.

Zhang, Q., Khan, M.U., Lin, X., Yi, W., Lei, H., 2020. Green-composites produced from waste residue in pulp and paperindustry: A sustainable way to manage industrial wastes. J. Clean. Prod.262, 121251. https://doi.org/10.1016/j.jclepro.2020.121251.

Acknowledgments

Authors acknowledge the staff at Electron Microscopy Service of the Universitat Politècnica de València for their support on the analysis of the samples. Authors wish to address a special thanks to the Company Gordon Confezioni srl (Cassano, Italy) for supplying the raw materials and for the contribution given to this research.

Authors thank the financial support of the Italian PRIN ("Progetto di Ricerca di Rilevante Interesse Nazionale) Project "SUSTAIN/ABLE – SimultaneoUs STructural And energetIc reNovAtion of BuiLdings through innovativE solutions", ERC Sector PE8, ID 20174RTL7W_007.